IEEE Access
Multidisciplinary | Rapid Review | Open Access Journal

SPECIAL SECTION ON EMERGING TECHNOLOGIES FOR ENERGY INTERNET

Received January 12, 2020, accepted February 5, 2020, date of publication February 10, 2020, date of current version February 26, 2020.

Digital Object Identifier 10.1109/ACCESS.2020.2972917

A Parameter-Exempted, High-Performance Power Decoupling Control of Single-Phase Electric Springs

QINGSONG WANG[1,2], (Senior Member, IEEE), ZHENGYONG DING[1], MING CHENG[1], (Fellow, IEEE), FUJIN DENG[1], (Member, IEEE), AND GIUSEPPE BUJA[3], (Life Fellow, IEEE)

[1]School of Electrical Engineering, Southeast University, Nanjing 210096, China
[2]Jiangsu Key Laboratory of Smart Grid Technology and Equipment, Zhenjiang 212000, China
[3]Department of Industrial Engineering, University of Padova, 35131 Padua, Italy

Corresponding author: Ming Cheng (mcheng@seu.edu.cn)

This work was supported in part by the Natural Science Foundation of Jiangsu Province under Project BK20170675, and in part by the National Natural Science Foundation of China under Project 51877040.

ABSTRACT Electric Spring (ES) is an emerging technology intended to stabilize the voltage across the critical load (CL) of an end-user in the presence of fluctuations of the grid power. The most advanced way of controlling the so-called second generation of ES relies on the handling of both active and reactive power. However, the strategies used to implement such a control suffer from either the need of an a-priori knowledge of circuit parameters or a slow response to the grid power fluctuations. In this paper, a control strategy is proposed that overcomes these inconveniences. It relies on two problem-solving solutions, namely the closed-loop control of the dq components of the current drawn by the end-user and a feedback of the ES output current into the ES command. The setup of the proposed power decoupling control has just the features of being no affected by the circuit parameters and exhibiting an enhanced dynamic behavior. The features are validated by both simulation and experimental results.

INDEX TERMS Electric spring, microgrid, power control, renewable energy source.

I. INTRODUCTION

Traditional power plants are increasingly being replaced or augmented by renewable energy sources (RESs) to contrast the carbon emissions. Unfortunately, the intermittent nature of the RESs is today the major cause of variations in the grid voltage and of the consequential breakdown in the voltage-sensitive (or critical) loads [1]–[3]. The electric spring (ES) is a cost-effective technology conceived several years ago to face this issue [4]. Let the critical load (CL) and the non-critical load (NCL) of an end-user be connected at a point of common coupling (PCC). When embedded in the NCL, an ES is able to stabilize the PCC voltage and, with it, the supply voltage of the CL. An ES for AC loads is also referred to as ACES.

Since the ES technology was proposed, many papers have appeared reporting on various ACES versions. The main versions are three. The first version, presented in [4], executes the voltage stabilization by enabling the ES to handle only reactive power. The second version, hereafter designated with ES-2, gives an ES the capability of handling the active and reactive powers [5]. Both the first and the second version insert the ES in series to the NCL. The third version, instead, inserts the ES in parallel to the NCL and the ES directly imposes the PCC voltage by handling again the active and reactive powers [6]. The versions above are also termed as ES generations since they are the milestones in the ES technology development. In addition to them, many other versions have been described [7]–[9]. Besides ACES, in recent times another kind of ES -referred to as DCES- has been studied to stabilize the supply voltage of the CLs connected to a DC microgrid [10], [11].

The associate editor coordinating the review of this manuscript and approving it for publication was Huiqing Wen.

Among the ACES versions, the ES-2 is considered in this paper since it is the most popular one; indeed, it offers the potential of controlling both the active and reactive power by means of a straightforward topology. So far, several strategies for the control of an ES-2 have been presented. The main strategies are as follows. In [5], the control principle with compensations of the active and reactive powers drawn by the NCL is analyzed at steady state. In [12], the so-called δ control is devised, built up around two closed loops: an inner loop for the control of the ES output current and an outer loop for the regulation of the PCC voltage. In [13], the radial-chordal decomposition (RCD) control of the PCC voltage vector is put forth, where the radial component determines the power angle of the branch constituted by the series of the ES and the NCL, commonly termed as smart load (SL), and the chordal component determines the magnitude of the PCC voltage. A number of control schemes are also discussed in the literature. However, almost all of them utilize the circuit parameters to deploy the control system. Furthermore, only a few focuses on the decoupled control of the active and reactive powers. This in spite of the fact that the fast-growing incidence of the power injected from RESs into the grid calls for the direct control of the active power drawn by the loads, according to the paradigm that the load demand has to follow the power generation.

Recently, a simple power decoupling (SPD) strategy for the active and reactive power control of an ES-2 application has been elaborated in [14]. The strategy has the inconvenience of a slow dynamic behavior. Moreover, although intuitive in conception and dispensing with the circuit parameters, it is lacking in the theoretical analysis for the selection of the control parameters. As a result, the trial-error approach has been adopted for their selection. To circumvent this approach, an analytical modeling of the end-user application with an ES-2 should be carried out, with the formulation of the transfer functions decoupling the actions of the active and reactive powers from the application outputs, but the ensuing implementation of the control still would require the knowledge of the circuit parameters.

The purpose of this paper is to develop a power decoupling control, which maintains the feature of a simple implementation that does not need the knowledge of the circuit parameters while, at the same time, is able to exhibit dynamics faster than the SPD control. This is achieved by setting up two current loops that regulate the line current drawn by the load on the d-axis and the q-axis, separately, and by complementing the loops with an active damping put in place through the feedback of the ES output current [15].

In detail, the paper is organized as follows. Section II reviews the operating principle of an ES-2 and discusses the main existing power control strategies. Section III expounds the theoretical bases of the proposed power decoupling control and explains the control diagram together with its operating functionalities. Section IV presents and discusses simulation and experimental results, the latter ones being measured from a lab ES-2 prototype operated with the proposed control. Finally, Section V concludes the paper.

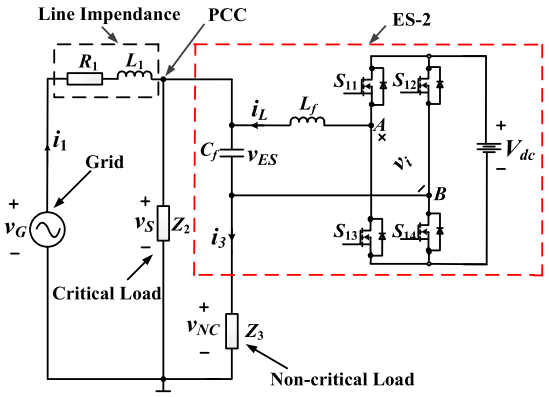

FIGURE 1. Single-phase ES-2 diagram application.

II. ES-2 TOPOLOGY AND POWER CONTROL STRATEGIES

A. ES-2 TOPOLOGY

The diagram of an ES-2 embedded in an end-user application is shown in Fig. 1, where the ES-2 is sketched within the dashed rectangle and contains a single-phase voltage-source inverter (VSI) [16], [17] and the LC low-pass filter represented by the pair L_f and C_f. In the figure, R_1 and L_1 are the resistance and the inductance of the distribution line, Z_2 and Z_3 are the impedances of the CL and the NCL, respectively, v_G is the grid voltage, v_S is the CL voltage coinciding with the PCC voltage, v_{NC} is the NCL voltage, i_1 is the grid current drawn by the end-user, also denoted as the input current, i_3 is the NCL current, i_L is the ES output current, and v_{ES} is the voltage across the capacitor C_f, also denoted as ES output voltage. It is worth to note that the suitable adjustment of v_{ES} is the key mechanism that stabilizes the PCC voltage against the grid voltage variations.

Voltage v_i in Fig. 1 is the VSI output voltage; the instantaneous amplitude of its fundamental component is proportional to the voltage V_{dc} of the DC source at the ES input as well as to the sinusoidal signal modulating v_i. The LC low-pass filter mitigates the high-frequency harmonics of v_i so that v_{ES} has a clean sinusoidal waveform.

B. ES-2 MODELING

Although the CL and the NCL can be of resistive, capacitive or inductive types, hereafter it is assumed that they are pure resistive to alleviate the complexity of the presentation. Thus, the state space equations of the ES-2 application in Fig. 1 take the following form:

$$\begin{cases} \dot{x} = Ax + Bu \\ y = Cx \end{cases} \tag{1}$$

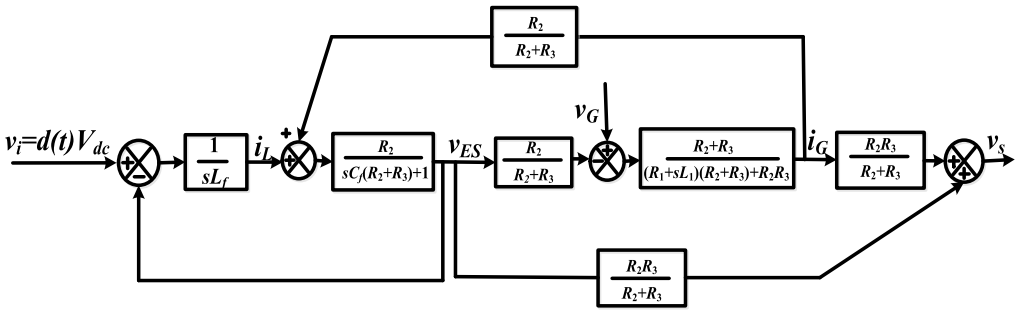

FIGURE 2. ES-2 application model.

where $x = \begin{bmatrix} i_L \\ v_{ES} \\ i_G \end{bmatrix}$, $u = \begin{bmatrix} v_G \\ v_i \end{bmatrix}$, $y = [v_s]$,

$$A = \begin{bmatrix} 0 & -\frac{1}{L_f} & 0 \\ \frac{1}{C_f} & -\frac{1}{C_f(R_2+R_3)} & \frac{R_2}{C_f(R_2+R_3)} \\ 0 & -\frac{R_2}{L_1(R_2+R_3)} & -\frac{R_1R_2+R_1R_3+R_2R_3}{L_1(R_2+R_3)} \end{bmatrix}$$

$$B = \begin{bmatrix} 0 & \frac{1}{L_f} \\ 0 & 0 \\ \frac{1}{L_1} & 0 \end{bmatrix}, \text{ and } C = \begin{bmatrix} 0 & \frac{R_2}{R_2+R_3} & \frac{R_2R_3}{R_2+R_3} \end{bmatrix}$$

Further to the equations above, the ES-2 application can be modeled as in Fig. 2. By disregarding the high-frequency harmonics, voltage v_i is expressed by $d(t)V_{dc}$, where $d(t)$ is the duty-cycle of the modulating signal. In the modeling process of the ES-2, they are also disregarded the dynamics of the DC source at the ES input.

C. EXISTING POWER CONTROL STRATEGIES

This Subsection discusses the power decoupling control strategies [12]–[14] anticipated in Section I.

1) δ CONTROL

The diagram of the δ control strategy is shown in Fig. 3(a) [12], where $\hat{\theta}$ is here the instantaneous phase of the grid voltage and the other quantities within the dashed rectangle labelled as δ control are defined in [12]. The strategy implements the power control by impressing the phase angle δ between the PCC and grid voltages. Such a value is calculated by manipulating the vectors of the AC electrical quantities in Fig. 1 with the purpose of meeting specified objectives. Besides the stabilization of the PCC voltage, the objective of operating the ES-2 under the constant active power or constant reactive power mode can be achieved. Therefore, the δ control strategy realizes the power decoupling control of the ES-2 with good dynamic performance. However, its operation relies on the modeling of the whole application, including the distribution line, and requires the a-priori knowledge of all the circuit parameters.

2) RCD CONTROL

The diagram of the RCD control strategy is shown in Fig. 3 (b) [13], where V_S and $\hat{\theta}$ are respectively the rms value and the instantaneous phase of the PCC voltage, ϕ_{SL_ref} is the reference of the SL impedance angle, ϕ_{i_ref} is the NCL impedance angle, and V_{esr} is the radial component of the ES voltage. Substantially, the RCD strategy keeps under control the magnitude of the voltage and the power angle of the SL by acting on the RCD components of the PCC voltage. The strategy has good dynamic performance and does not utilize either the line impedance or the CL parameters but still needs the NCL parameters.

3) SPD CONTROL

The diagram of the SPD control strategy is shown in Fig. 3 [14], where P_{in} and Q_{in} are the active and reactive powers drawn by the ES-2 application. They are compared with the respective references and then processed by separate Proportional Integral (PI) controllers to deliver the dq commands of v_{ES}. The references of P_{in} and Q_{in} are set respectively to meet a specified objective and to regulate the PCC voltage, and the PI coefficients are tuned by the trial-error approach. The bandwidths of the power loops are constrained to be somewhat low to prevent the onset of instability phenomena, thus slowing down the application dynamics.

The analysis above points out that the existing power control strategies are either intricate or sluggish so that it appears of interest the development of a control solution that is both simple and dynamics-effective.

III. PROPOSED ES-2 POWER DECOUPLING CONTROL

This paper continues on the way traced in [14] by proposing a SPD control of an ES-2 that combines the feature of an implementation little affected by the circuit parameters to that of a behavior with fast dynamics. Instrumental in the proposal is the transformation of the single-phase variables in a dq rotating reference frame.

A. SINGLE-PHASE dq-AXIS POWERS

The dq transformation is commonly used in the three-phase systems. In order to use it in the single-phase systems the

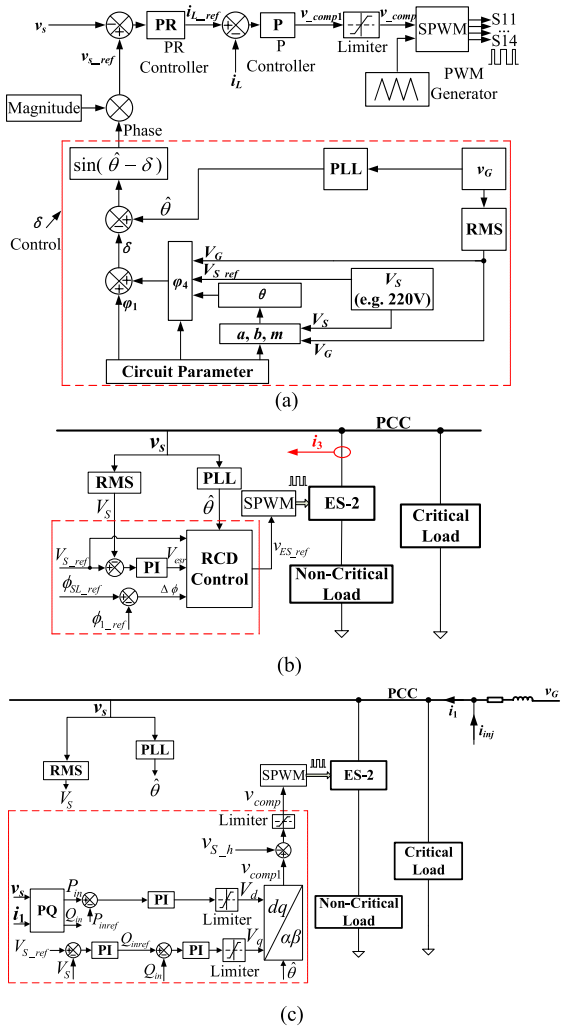

FIGURE 3. ES-2 power decoupling control strategies. (a) δ control [12]. (b) RCD control [13]. (c) SPD control [14].

virtual orthogonal components of the single-phase quantities must be made available. There are many methods to work them out: for instance, the 1/4T delay method, the differential method, the secondorder generalized integrator (SOGI) algorithm [18] and so on. In this paper, the SOGI algorithm is utilized because of its steady-state and transient accuracy.

Let us consider only the fundamental components of the AC quantities in the diagram of Fig. 1, and let us assume that, under enough slow dynamics, they are represented by sinusoidal expressions. By selecting the PCC voltage vector $\boldsymbol{V_S}$ as a reference, the voltage and current at PCC can be written as

$$v_s(t) = \sqrt{2}V_s\cos(\omega t) \tag{2}$$
$$i_1(t) = \sqrt{2}I_1\cos(\omega t + \phi) \tag{3}$$

and the vectors $\boldsymbol{V_s}$ and $\boldsymbol{I_1}$ as

$$\boldsymbol{V_s} = V_s\angle 0 = V_s \tag{4}$$
$$\boldsymbol{I_1} = I_1\angle\phi = I_1(\cos\phi + j\sin\phi) \tag{5}$$

In the $\alpha\beta$ stationary frame, the voltage vector $\boldsymbol{v_{s\alpha\beta}}$ and the current vector $\boldsymbol{i_{1\alpha\beta}}$ are expressed as

$$\boldsymbol{v_{s\alpha\beta}} = \begin{bmatrix} v_{s\alpha} \\ v_{s\beta} \end{bmatrix} = V_s\begin{bmatrix} \cos(\omega t) \\ \sin(\omega t) \end{bmatrix} \tag{6}$$
$$\boldsymbol{i_{1\alpha\beta}} = \begin{bmatrix} i_{G\alpha} \\ i_{G\beta} \end{bmatrix} = I_1\begin{bmatrix} \cos(\omega t + \phi) \\ \sin(\omega t + \phi) \end{bmatrix} \tag{7}$$

The transformation matrix T that converts a quantity from the $\alpha\beta$ stationary frame to the dq reference frame rotating in synchronism with the PCC voltage is given by

$$\mathrm{T} = \begin{bmatrix} \cos(\omega t) & \sin(\omega t) \\ -\sin(\omega t) & \cos(\omega t) \end{bmatrix} \tag{8}$$

By (8), the voltage vector $\boldsymbol{v_{sdq}}$ and the current vector $\boldsymbol{i_{1dq}}$ in the dq rotating reference frame are calculated as in (9) and (10).

$$\boldsymbol{v_{sdq}} = \begin{bmatrix} v_{sd} \\ v_{sq} \end{bmatrix} = T\begin{bmatrix} v_{s\alpha} \\ v_{s\beta} \end{bmatrix} = V_s\begin{bmatrix} 1 \\ 0 \end{bmatrix} \tag{9}$$
$$\boldsymbol{i_{1dq}} = \begin{bmatrix} i_{Gd} \\ i_{Gq} \end{bmatrix} = T\begin{bmatrix} i_{G\alpha} \\ i_{G\beta} \end{bmatrix} = I_1\begin{bmatrix} \cos\phi \\ \sin\phi \end{bmatrix} \tag{10}$$

Thus, the vector expressions of $\boldsymbol{V_s}$ and $\boldsymbol{I_1}$ in the dq rotating reference frame are given by

$$\boldsymbol{V_s} = V_s\angle 0 = V_s = v_{sd} + jv_{sq} \tag{11}$$
$$\boldsymbol{I_1} = I_1\angle\phi = I_1(\cos\phi + j\sin\phi) = i_{1d} + i_{1q} \tag{12}$$

From (9)-(11), the active power P_{in} and the reactive power Q_{in} entering into the load are expressed as

$$\begin{aligned} P_{in} &= \mathrm{Re}\left(\boldsymbol{V_s}\boldsymbol{I_1^*}\right) = \mathrm{Re}\left(\left\{v_{sd} + jv_{Sq}\right\}\cdot\left\{i_{1d} + ji_{1q}\right\}\right) \\ &= v_{Sd}i_{1d} + v_{Sq}i_{1q} = v_{Sd}i_{1d} = V_SI_1\cos\phi \end{aligned} \tag{13}$$
$$\begin{aligned} Q_{in} &= \mathrm{Im}\left(\boldsymbol{V_s}\boldsymbol{I_1^*}\right) = \mathrm{Im}\left(\left\{v_{sd} + jv_{sq}\right\}\cdot\left\{i_{1d} + ji_{1q}\right\}\right) \\ &= v_{Sq}i_{1d} - v_{Sd}i_{1q} = -v_{Sd}i_{1q} = V_SI_1\sin\phi \end{aligned} \tag{14}$$

Here i_{1d} and i_{1q} represent the active and reactive components of the input current, respectively.

B. PROPOSED CONTROL DIAGRAM

The diagram of the proposed power decoupling control of the ES-2 is illustrated within the dashed rectangle of Fig. 4. In the figure, $i_{1\alpha}$ coincides with i_1 whilst $i_{1\beta}$ lags i_1 by 90°, and i_{1d} and i_{1q} are the currents at the output of the $\alpha\beta$ to dq transformation. The references of the currents i_{1d} and i_{1q} are delivered by the PI controllers of the active and reactive powers P_{in} and Q_{in}; in particular, the PI controller closing the active power loop delivers the reference of the current i_{1d} whilst that one closing the active power loop delivers the reference of the current i_{1q}. In turn, the currents i_{1d} and i_{1q} are processed by PI controllers to deliver the dq references of v_{ES}. Before commanding the ES-2, they are transformed back to the $\alpha\beta$ stationary frame and generate the signal v_{comp1} modulating the VSI output voltage. The current loops inner to those of power help enlarging the bandwidth of the ES-2 application since they override the delays in the current control paths. Therefore, the dynamics of the application

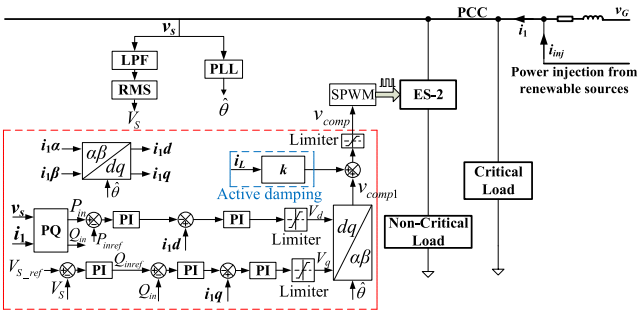

FIGURE 4. The proposed power control on ES-2.

become faster than in [14]. As a return, the transients further to a change of the power references decay with persistent oscillations. To achieve a damped response, the ES output current is entered into the command path of the ES voltage after multiplication by the gain k, acting as a current feedback. It is added to the signal v_{comp1} so as to contribute to the signal v_{comp} used to modulate the VSI output voltage. It should be noted that the proposed control cannot work effectively without the ES output current both in our simulations and experiments.

C. PROPOSED CONTROL MERITS

A brief comparison between the proposed power decoupling control and that one described in [14] discloses that both have the merit to be simple since they do not rely on the circuit parameters. Additionally, the proposed control has the merit of improving the dynamics of the ES-2 application because of the larger control bandwidth. Besides, it offers the way of designing the control system by taking advantage of the modeling of the application.

IV. SIMULATIONS

For a first validation of the proposed power decoupling control, simulations have been carried out in the MATLAB/Simulink environment. Parameters of the application are provided in Table 1. In the simulations and experiments, the PI parameters are tuned using trial and error due to the absence of system modeling, and the damping gain k is chosen as -0.67.

The simulations refer to an ES-2 application supplied by both a traditional grid and a RES through a grid-tied converter (GCC). They and are organized in two steps: in the first step, only the ES-2 is activated; in the second step the GCC is also activated and injects the current i_{inj} into the PCC.

A. ONLY ES-2 ACTIVATION

In this Subsection, only the ES-2 is activated. The simulation diagram is sketched in Fig. 5 where, as an example, v_G is fixed at 200 V.

The responses of various quantities of the ES-2 application to variations of P_{inref} are traced in the Figs. 6(a) and (b). Specifically, P_{inref} is set to 4 kW from 0 to 0.4 s; then it is stepped down to 2 kW from 0.4 to 0.8 s and finally to 1 kW

TABLE 1. Parameters for simulations.

Items	Values
PCC voltage (V_S)	220V
DC bus voltage (V_{dc})	400V
Line resistance (R_1)	1Ω
Line inductance (L_1)	24mH
Inductance of filter inductor (L_2)	26mH
Critical load (Z_2)	44Ω
Non-critical load (Z_3)	14.7Ω
Inductance of ES filter (L_f)	3mH
Capacitance of ES filter (C_f)	50μF
ES Switching frequency (f_s)	20kHz

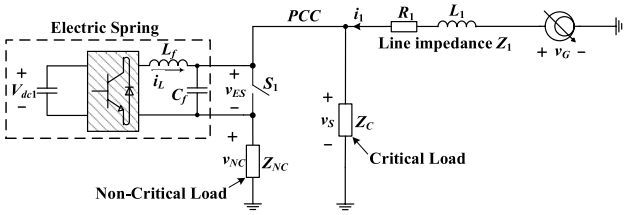

FIGURE 5. ES-2 application simulation diagram.

from 0.8 to 1.2 s. Meanwhile, Q_{inref} is kept constant at 1 kVar from 0 to 1.2 s. The upper graph of the Fig. 6(a) gives the voltage grid. The other graphs report the responses of P_{in}, Q_{in} and the CL rms voltage. To illustrate the overall effects of the control on the ES-2 application, the Fig. 6 (b) reports the responses of other quantities, namely the active powers drawn by the CL, the ES-2, and the NCL, respectively; as a reference, the first graph repeats the trace of P_{in}. The graphs show that P_{in} tracks P_{inref} quickly, settling at the reference value with no error, and that Q_{in} is regulated around Q_{inref} with no error in steady-state. Moreover, they show that the active power drawn by the CL is kept nearly constant at its nominal value of 860 W while the active powers drawn by the ES-2 and the NCL vary in the same way as P_{in}.

In the Fig. 6(c), Q_{inref} is set to 3kVar during 0 to 0.4s; then it is stepped down to 1.5kVar from 0.4 to 0.8s and finally to 0.5kVar from 0.8 to 1.2s. Meanwhile, P_{inref} is kept constant at 2kW. The steady-state and dynamic behaviors of the ES-2 application is as effective as in the previous case, provided that the responses of P_{in} and Q_{in} are exchanged each other.

In the Fig. 7, v_G is added with the third harmonic components at 0.4s and added with the fifth harmonic components at 0.8s, 30V and 20V, respectively. Simulation results indicate that the input active and reactive powers of ES system are regulated well to follow the predefined values under the condition of grid distortion.

The simulation results reveal that the proposed power decoupling control is both accurate in stationary conditions and very performing during the transients of the active and

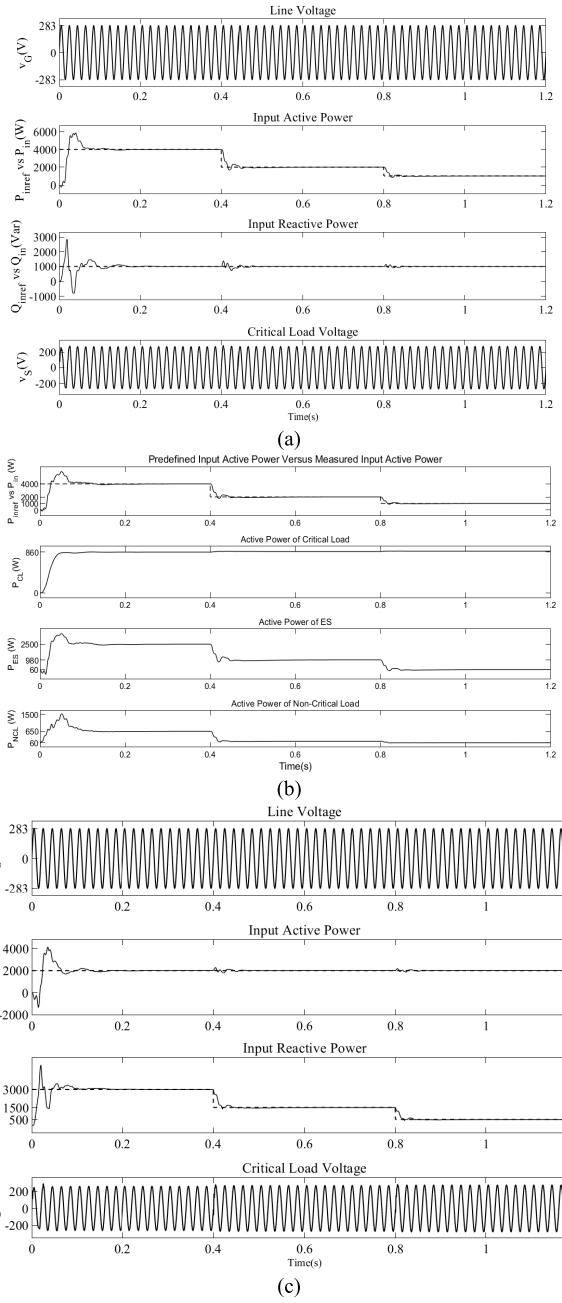

FIGURE 6. ES-2 application simulation responses; (a) input powers and CL rms voltage, and (b) CL, NCL and ES powers, both under variations of P_{inref}, (c) input powers and CL rms voltage under variations of Q_{inref}.

reactive powers. Besides, the proposed control is immune to the influence of the grid harmonics.

B. JOINT ES-2 AND GCC ACTIVATION

In this subsection, both the ES-2 and the GCC are activated. The simulation diagram is sketched in Fig. 8 and the simulation results are reported in the Figs. 9(a)-(d). These figures are composed of six graphs and give respectively the PCC voltage versus the GCC-injected current i_{inj}, the power generated by

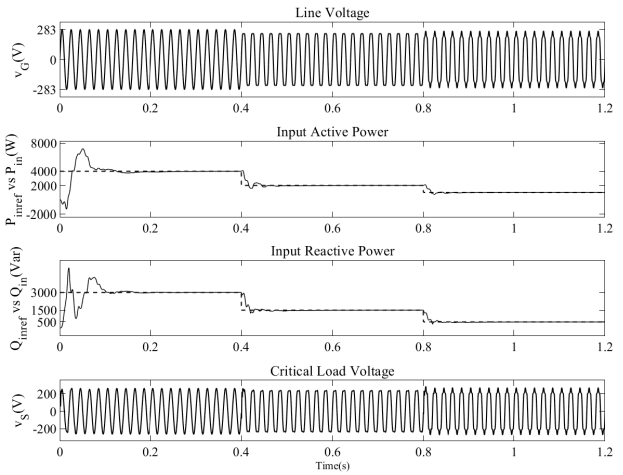

FIGURE 7. Simulation waveforms under the condition of grid distortion.

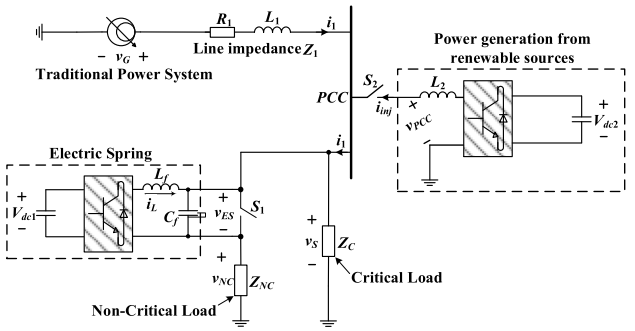

FIGURE 8. Simulation diagram of the ES application with grid-tied GCC.

the RES, and the powers entering into the grid, the CL, the NCL, and the ES-2, respectively.

Fig. 9(a) traces the above-mentioned quantities in response to variations of i_{inj}. The corresponding injected power starts from a value of 2600 W, then is stepped up to 3500 at 0.6s and finally to 4400 at 1.2s. Figs. 9(b)-(d) are a zoom of the Fig. 9(a). In detail, Fig. 9(b) traces the quantities when i_{inj} is 12A while Figs. 9(c) and (d) trace them along the time intervals where i_{inj} is 16A and 20A. The traces indicate that the powers drawn by the grid and the CL remain constant at 1100 W despite the variations of the power injected by the RES. As it emerges from the graphs, the latter ones are passed to the NCL and the ES, thus confirming the capability of the control in properly managing the grid power fluctuations.

V. EXPERIMENTS AND DISCUSSIONS

For the experimental validation of the proposed power decoupling control, a feasibility study has been carried out on a laboratory setup, empowered with a 300W PWM rectifier in the DC side of the ES-2 to emulate a bidirectional voltage source, as depicted in the Figs. 10(a) and (b) In this situation, large line resistance and line inductance values are chosen to help limit the power rating of the system which should match the rated power capacity of the PWM rectifier. Besides, it should be noted that the voltage of PWM rectifier must

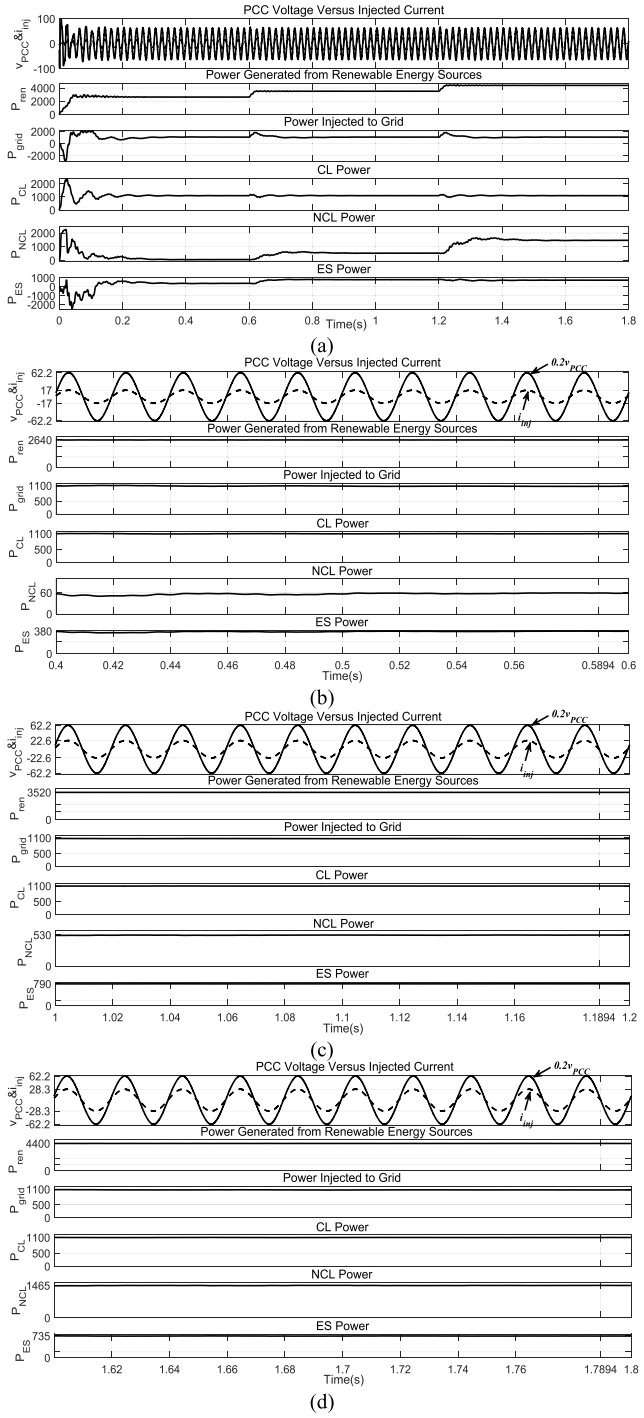

FIGURE 9. Simulation waveforms under injection of different values of i_{inj}. (a) overview of ES-2 application responses; (b)-(d) interval zooms: (b) for i_{inj} =12A. (c) for i_{inj} =16A. (d) for i_{inj} =20A.

match the voltage level of the system. For instance, the DC bus voltage should be larger than 77.77V in the 55V experimental platform.

A. ONLY ES-2 ACTIVATION

Before proceeding to the experimentation of the control setup, the dynamic performance of the current loops are tested since a fast responses of them is a prerequisite for succeeding in speeding up the power loops.

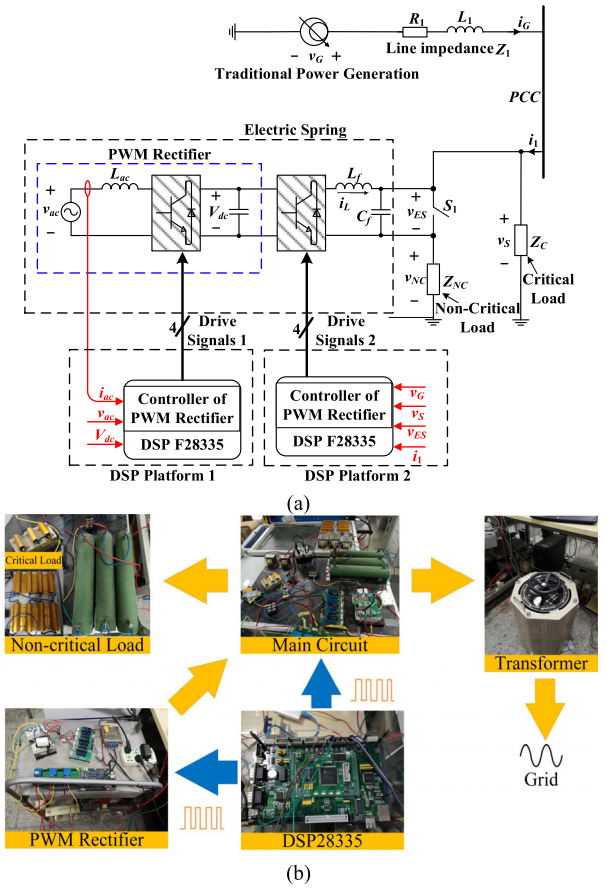

FIGURE 10. Experimental setup. (a) Implementation diagram. (b) Stage pictures.

TABLE 2. Parameters for experiments.

Items	Values
PCC voltage (V_S)	55V
DC bus voltage (V_{dc})	100V
Line resistance (R_1)	1.64Ω
Line inductance (L_1)	30.4mH
Critical load (Z_2)	1603.4Ω
Non-critical load (Z_3)	51.05Ω
Inductance of ES filter (L_f)	2.3mH
Capacitance of ES filter (C_f)	26μF
ES Switching frequency (f_s)	20kHz

Figs. 11(a) and (b) show the experimental results obtained for the current responses. In Fig. 11(a), i_{dref} is stepped up from 0.5 to 2A while i_{qref} is kept at 0. In Fig. 11(b), i_{dref} is kept at 1A while i_{qref} is stepped up from 0 to 1A. The traces in the Fig. 11(a) indicate that i_d settles to its reference value in 0.12s while i_q is influenced by the step of i_{dref}; however, the deviation from its reference value is small and runs out in 12s as well; in turn, the traces in the Fig. 11(b) indicate a

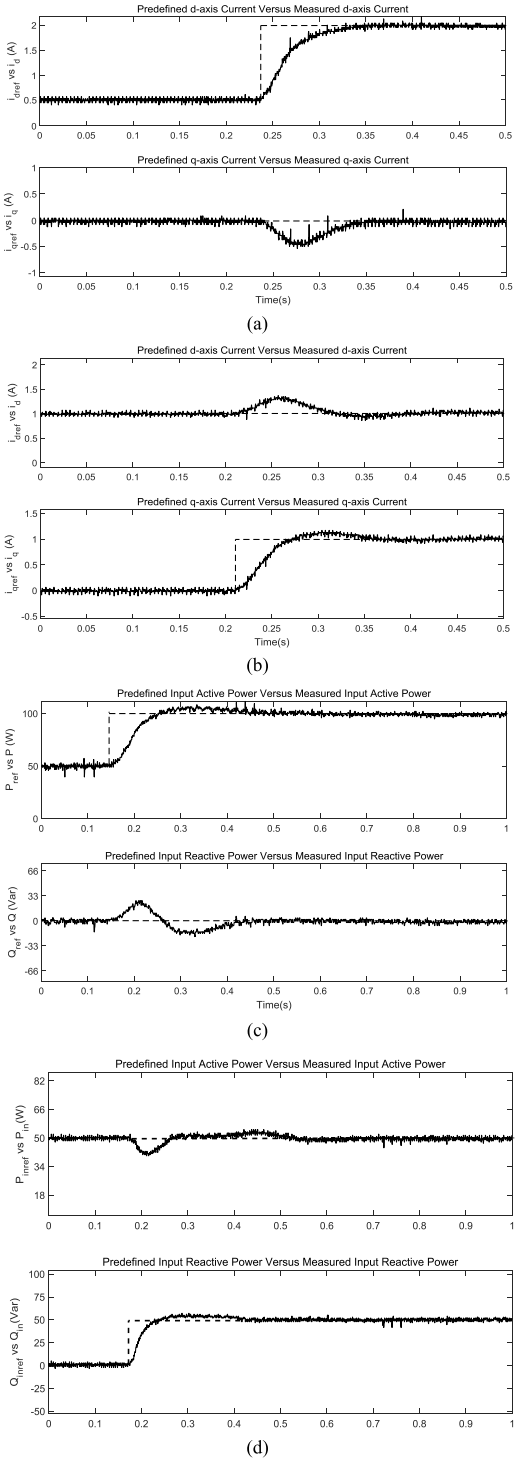

FIGURE 11. Experimental responses to (a) i_{dref} steps from 0.5 to 2A with i_{qref} kept at 0A. (b) i_{qref} steps from 0 to 1A with i_{dref} kept at 1A. (c) P_{inref} steps from 50 to 100W with Q_{inref} kept at 0Var. (d) Q_{inref} steps from 0 to 50Var with P_{inref} kept at 50W.

dual behavior for i_q and i_d, apart from a little higher settling time of 0.15s. In either case, the traces demonstrate that the fast dynamics of the current responses.

Lastly, the effectiveness of the whole power decoupling control is tested. The experimental results are reported in the

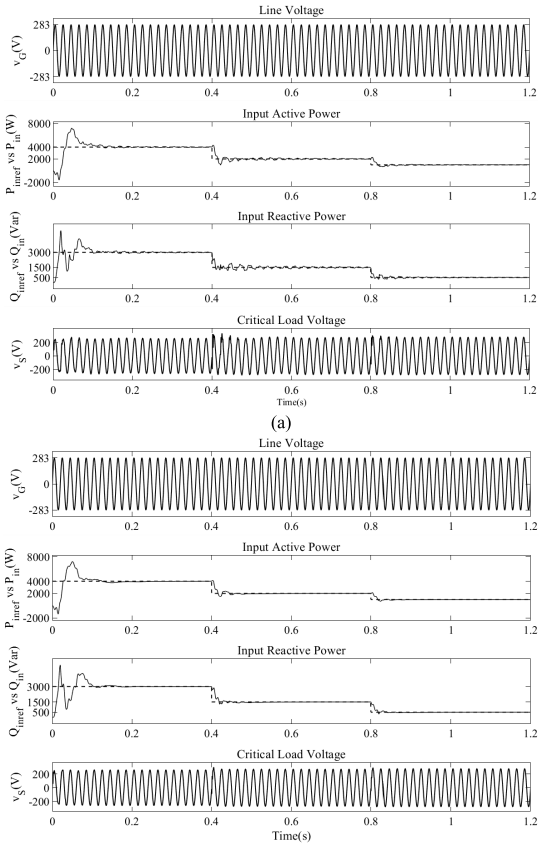

FIGURE 12. ES-2 application simulation responses; (a) SPD control (b) proposed control.

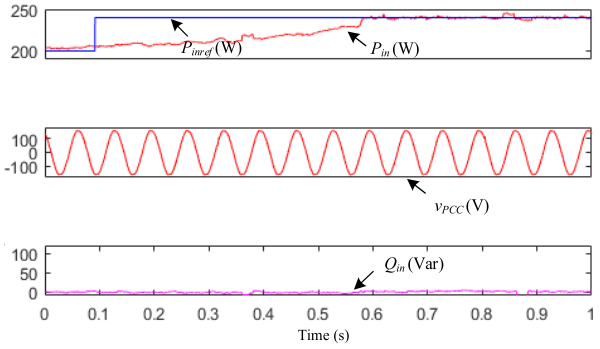

FIGURE 13. Experimental responses to P_{inref} variation from 200 to 240W with control in [14].

Figs. 11(c) and (d). In the Fig. 11(c), P_{inref} is set to 50W from 0 to 0.14s and then stepped up to 100W from 0.14 to 1s. Meanwhile, Q_{inref} is kept at 0. It can be observed that P_{in} tracks the reference in 0.36s with a well-damped behavior and that Q_{in} undergoes a certain deviation that settles down in an equal time with an equally well-damped behavior. In the Fig. 11(d), Q_{inref} is set to 0Var from 0 to 0.18s and then stepped up to 50Var from 0.18 to 1s. Meanwhile, P_{inref} is kept at 50W. It can be observed that the dynamics of P_{in} and Q_{in} are the dual of the previous test, the only difference being a little shorter settling time of 0.32s.

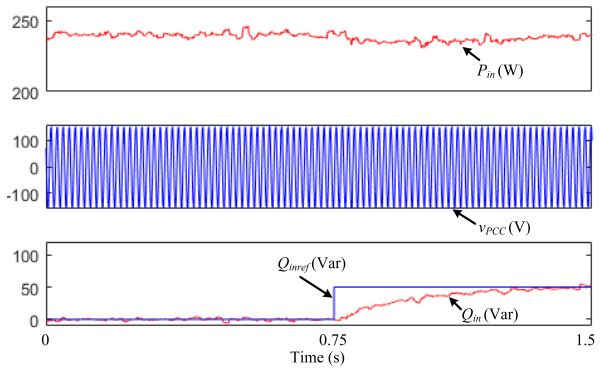

FIGURE 14. Experimental responses to Q_{inref} variation from 0 to 50Var with control in [14].

B. COMPARISONS WITH EXISTING POWER DECOUPLING CONTROL

In simulations, the PI parameters of the power loops are set to the same for a relatively fair comparison. When the predefined values of active power and reactive power vary at the same time, active power and reactive power can trace the predefined value quickly under the proposed control, while simple active and reactive power control costs more than 0.1s to reach the targets in Figure. 12.

In experiments, with the control in [14], P_{in} takes 0.5s to change from 200 to 240 W and Q_{in} takes 0.75s to change from 0 to 50 Var in response to the same steps of the respective references, as shown in Figs. 13 and 14. Instead, the proposed control spends only 0.36s and 0.32s to reach the targets, thus confirming its enhanced dynamics.

C. DISCUSSIONS

The experimental results have proven that the dynamic responses of the proposed control is somewhat faster than that in [14]. This agrees with the prediction that the inner current loops would have extended the bandwidths of the power loops. The setup of the control system is not affected by the circuit parameters, which means that it can be transferred to more complicated end-user applications. On the other hand, the dynamics of the active and reactive powers are not decoupled each other completely so that the change in the reference of one of them produces a transient deviation of the other one. However, the deviations are acceptable as they are small in amplitude and vanish as quick as the dynamics of the changed power.

VI. CONCLUSION

This paper has proposed, explicated and validated a power decoupling control for an ES-2 in applications such as the households supplied by microgrids. Compared to the existing power decoupling control in [14], the dynamic responses of the power loops have been made faster thanks to the introduction of current loops in the *dq* rotating reference frame while the control setup is still simple as it does not need the circuit paraments. To enable the *dq*-axis modeling of the ES-2 application, the virtual orthogonal signals of the voltage and current at PCC have been extracted by exploiting the SOGI algorithm. As one of the control objectives of the ES-2 is the stabilization of the PCC voltage the vector of such a voltage has been selected as the reference for the *dq* transformation, helping decomposing the grid current entering into the PCC in the active and reactive components. By help of this decomposition, the decoupling control of the active and reactive powers has been achieved utilizing PI controllers. Finally, the effectiveness of the proposed control is validated by both simulation and experimental results.

REFERENCES

[1] C. Xie, K. Li, J. Zou, and J. M. Guerrero, "Passivity-based stabilization of LCL-type grid-connected inverters via a general admittance model," *IEEE Trans. Power Electron.*, to be published, doi: 10.1109/tpel.2019.2955861.
[2] H. Hu, P. Pan, Y. Song, and Z. He, "A novel controlled frequency band impedance measurement approach for single-phase railway traction power system," *IEEE Trans. Ind. Electron.*, vol. 67, no. 1, pp. 244–253, Jan. 2020.
[3] H. Hu, Y. Shao, L. Tang, J. Ma, Z. He, and S. Gao, "Overview of harmonic and resonance in railway electrification systems," *IEEE Trans. Ind. Appl.*, vol. 54, no. 5, pp. 5227–5245, Sep./Oct. 2018.
[4] S. Y. Hui, C. K. Lee, and F. F. Wu, "Electric springs—A new smart grid technology," *IEEE Trans. Smart Grid*, vol. 3, no. 3, pp. 1552–1561, Sep. 2012.
[5] S.-C. Tan, C. K. Lee, and S. Y. Hui, "General steady-state analysis and control principle of electric springs with active and reactive power compensations," *IEEE Trans. Power Electron.*, vol. 28, no. 8, pp. 3958–3969, Aug. 2013.
[6] C. K. Lee and S. Y. R. Hui, "Input AC voltage control bi-directional power converters," U.S. Patent 13 907 350 A1, May 31, 2013.
[7] S. Yan, M.-H. Wang, T.-B. Yang, S.-C. Tan, B. Chaudhuri, and S. Y. R. Hui, "Achieving multiple functions of three-phase electric springs in unbalanced three-phase power systems using the instantaneous power theory," *IEEE Trans. Power Electron.*, vol. 33, no. 7, pp. 5784–5795, Jul. 2018.
[8] Z. Akhtar, B. Chaudhuri, and S. Y. R. Hui, "Smart loads for voltage control in distribution networks," *IEEE Trans. Smart Grid*, vol. 8, no. 2, pp. 937–946, Mar. 2017.
[9] Q. Wang, M. Cheng, and Y. Jiang, "Harmonics suppression for critical loads using electric springs with current-source inverters," *IEEE J. Emerg. Sel. Topics Power Electron.*, vol. 4, no. 4, pp. 1362–1369, Dec. 2016.
[10] Q. Wang, D. Zha, F. Deng, M. Cheng, and G. Buja, "A topology of DC electric springs for DC household applications," *IET Power Electron.*, vol. 12, no. 5, pp. 1241–1248, May 2019.
[11] M.-H. Wang, K.-T. Mok, S.-C. Tan, and S. Y. R. Hui, "Multifunctional DC electric springs for improving voltage quality of DC grids," *IEEE Trans. Smart Grid*, vol. 9, no. 3, pp. 1552–1561, May 2018.
[12] Q. Wang, M. Cheng, and Z. Chen, "Steady-state analysis of electric springs with a novel δ control," *IEEE Trans. Power Electron.*, vol. 30, no. 12, pp. 7159–7169, Dec. 2015.
[13] K.-T. Mok, S.-C. Tan, and S. Y. R. Hui, "Decoupled power angle and voltage control of electric springs," *IEEE Trans. Power Electron.*, vol. 31, no. 2, pp. 1216–1229, Feb. 2016.
[14] Q. Wang, M. Cheng, Y. Jiang, W. Zuo, and G. Buja, "A simple active and reactive power control for applications of single-phase electric springs," *IEEE Trans. Ind. Electron.*, vol. 65, no. 8, pp. 6291–6300, Aug. 2018.
[15] C. Xie, X. Zhao, K. Li, J. Zou, and J. M. Guerrero, "A new tuning method of multiresonant current controllers for grid-connected voltage source converters," *IEEE J. Emerg. Sel. Topics Power Electron.*, vol. 7, no. 1, pp. 458–466, Mar. 2019.
[16] M.-H. Wang, S. Yan, S.-C. Tan, and S. Y. Hui, "Hybrid-DC electric springs for DC voltage regulation and harmonic cancellation in DC microgrids," *IEEE Trans. Power Electron.*, vol. 33, no. 2, pp. 1167–1177, Feb. 2018.
[17] Y. Wang, Z. Chen, X. Wang, Y. Tian, Y. Tan, and C. Yang, "An estimator-based distributed voltage-predictive control strategy for AC islanded microgrids," *IEEE Trans. Power Electron.*, vol. 30, no. 7, pp. 3934–3951, Jul. 2015.
[18] R. Zhao, Z. Xin, P. C. Loh, and F. Blaabjerg, "A novel flux estimator based on multiple second-order generalized integrators and frequency-locked loop for induction motor drives," *IEEE Trans. Power Electron.*, vol. 32, no. 8, pp. 6286–6296, Aug. 2017.

QINGSONG WANG (Senior Member, IEEE) received the B.Sc. and M.Sc. degrees from the Department of Electrical Engineering, Zhejiang University, Hangzhou, China, in 2004 and 2007, respectively, and the Ph.D. degree from the School of Electrical Engineering, Southeast University, Nanjing, China, in 2016.

From July 2004 to July 2005, he was an Engineer with Shihlin Electronic & Engineering Company, Ltd., Suzhou, China. From July 2007 to August 2011, he was an Engineer with the Global Development Center, Philips Lighting Electronics, Shanghai, China. In October 2010, he was promoted to be a Senior Engineer. From August 2011 to September 2013, he was a Lecturer with the PLA University of Science and Technology, Nanjing. From November 2015 to November 2016, he was a joint Ph.D. Student with the Department of Energy Technology, Aalborg University, Aalborg, Denmark, where he focused on electric springs. Since 2017, he has been with Southeast University, where he is currently a Lecturer with the School of Electrical Engineering. He is also with the Jiangsu Key Laboratory of Smart Grid Technology and Equipment. His research interest is focused on the area of control and applications of power electronics to power systems.

ZHENGYONG DING received the B.Sc. degree from the Nanjing University of Aeronautics and Astronautics, Nanjing, China, in 2018. He is currently pursuing the M.Eng. degree with the School of Electrical Engineering, Southeast University, Nanjing.

His current research interest includes applications of power electronics to power systems.

MING CHENG (Fellow, IEEE) received the B.Sc. and M.Sc. degrees from the Department of Electrical Engineering, Southeast University, Nanjing, China, in 1982 and 1987, respectively, and the Ph.D. degree from the Department of Electrical and Electronic Engineering, The University of Hong Kong, Hong Kong, in 2001.

Since 1987, he has been with Southeast University, where he is currently a Professor with the School of Electrical Engineering and the Director of the Research Center for Wind Power Generation. His teaching and research interests include electrical machines, motor drives for electric vehicles, and renewable energy generation. He has authored or coauthored over 300 technical articles and four books. He is the holder of 55 patents in these areas.

Dr. Cheng is a Fellow of the Institution of Engineering and Technology (IET). He has served as the Chair and an Organizing Committee Member for many international conferences. He is also a Distinguished Lecturer of the IEEE Industry Applications Society (IAS), in 2015 and 2016.

FUJIN DENG (Member, IEEE) received the B.Eng. degree in electrical engineering from the China University of Mining and Technology, Jiangsu, China, in 2005, the M.Sc. degree in electrical engineering from Shanghai Jiao Tong University, Shanghai, China, in 2008, and the Ph.D. degree in energy technology from the Department of Energy Technology, Aalborg University, Aalborg, Denmark, in 2012. From 2013 to 2015 and 2015 to 2017, he was a Postdoctoral Researcher and an Assistant Professor with the Department of Energy Technology, Aalborg University, respectively. He joined Southeast University, Nanjing, China, in 2017, where he is currently a Professor with the School of Electrical Engineering. His main research interests include wind power generation, multilevel converters, high-voltage direct-current (HVDC) technology, dc grid, and offshore wind farm-power systems dynamics.

GIUSEPPE BUJA (Life Fellow, IEEE) received the Laurea degree (Hons.) in power electronics engineering from the University of Padova, Padua, Italy.

He is currently a Full Professor with the University of Padova. He has carried out an extensive research work in the field of power and industrial electronics, originating the modulating-wave distortion and the optimum modulation for pulse-width modulation inverters, pioneering the introduction of digital signal processing in the control systems of power electronics converters, and conceiving advanced techniques for the control of electric drives. His current research interests are automotive electrification, including wireless charging of electric vehicles and grid-integration of renewable energies. He is currently a member of the Editorial Board of the *Chinese Journal of Electrical Engineering* and a Senior Member of the Administrative Committee of the IES. He received the IEEE Industrial Electronics Society (IES) Eugene Mittelmann Achievement Award in recognition of his outstanding technical contributions to the field of industrial electronics and the 2016 Best Paper Award from the IEEE TRANSACTIONS ON INDUSTRIAL ELECTRONICS. He has served on the IEEE in several capacities, including as the General Chairman for the 20th Annual Conference of the IES (IECON), in 1994. He is also an Associate Editor of the IEEE TRANSACTIONS ON INDUSTRIAL ELECTRONICS.